INTERNATIONAL JOURNAL FOR NUMERICAL METHODS IN FLUIDS, VOL. 25, 1137–1161 (1997)

A BOUNDED CONVECTION SCHEME FOR THE OVERLAPPING CONTROL VOLUME APPROACH

ATUL KUMAR VERMA AND V. ESWARAN*

Department of Mechanical Engineering, Indian Institute of Technology, Kanpur 208 016, India

SUMMARY

This paper introduces a flux-limited scheme FLOCV for the overlapping control volume (OCV) approach to 2D steady and unsteady convection–diffusion problems on structured non-orthogonal grids. FLOCV switches from second- to first-order interpolation in the presence of extrema. Smooth switching between the two is ensured by weighted average second- and first-order upwind differencing, with the weights being dynamically determined. Five convective test problems are solved using this scheme and results are compared with known analytical solutions. It is found that FLOCV approximately retains second-order accuracy of the base discretization scheme on uniform grids and smooth non-uniform orthogonal grids. It is also found effective in removing oscillations for problems with discontinuities on both orthogonal and non-orthogonal grids, with little degradation of accuracy.

Int. J. Numer. Meth. Fluids, **25**: 1137–1161 (1997)

No. of Figures: 6. No. of Tables: 15. No. of References: 23.

KEY WORDS: flux limiters; FLOCV; overlapping control volume; finite volume method; convection–diffusion; structured non-orthogonal grid

1. INTRODUCTION

A major difficulty in numerically modelling flow equations is in discretizing the convective term. A good scheme should possess the following properties: accuracy, stability, boundedness and algorithmic simplicity. These requirements are often in opposition to one another. Stability and boundedness require that the scheme have diffusive smoothing, whereas accuracy suffers by this. Simple upwinding, although stable and bounded, introduces 'numerical diffusion'. In problems with strong flow-to-grid skewness, first-order upwind schemes are unsatisfactory because of their highly diffusive nature. Higher-order schemes (e.g. QUICK of Leonard,[1] OCV of Verma and Eswaran,[2] etc.) are able to reduce the level of cross-wind diffusion significantly for oblique flows. However, they produce unphysical oscillations in regions of strong gradients. Just as numerical dissipation dominates the error in first-order schemes, dispersion, which causes oscillations, may be significant in second-order ones. We discuss below schemes that have been used to reduce oscillations in the solutions of a *single-scalar* convective equation, though many of these schemes have been used in other circumstances.

Correspondence to: V. Eswaran, Department of Mechanical Engineering, Indian Institute of Technology, Kanpur 208 016, India.

CCC 0271–2091/97/101137–25 $17.50

Received April 1996
Revised February 1997

Spurious oscillations may be suppressed by adding viscosity artificially to the scheme[3] or smoothing the solution after each timestep. Another approach, that of non-linear limiters, aims at preventing the generation of numerical oscillations instead of damping them after they have been generated. The flux-corrected transport (FCT) scheme of Boris and Book[4] was the first attempt to develop a higher-order monotonic scheme. Zalesak[5] has modified and enhanced the FCT scheme.

The total-variation-diminishing (TVD) schemes introduced by Harten[6] are designed to ensure that the total variation, i.e. the sum of the magnitude of differences in the solution between adjacent grid points, always decreases in the solution. Some other schemes in this class are the ENO (essentially non-oscillatory) schemes of Shu and Osher,[7] the slope modification method of Yang[8] and the TVD scheme of Wang and Windhopf.[9] Hirsch[10] provides extensive reviews of TVD schemes and other high-order schemes.

Many schemes have been developed to eliminate oscillations in practical multidimensional flow equations and are tested on the convection–diffusion equation. The bases of evaluating such schemes are generally (a) boundedness, i.e. that the scheme eliminates spurious oscillations, (b) minimal diffusion, i.e. that it does not *spread* the solution by introducing too much diffusion, (c) accuracy, i.e. that it does not cause too great a degradation of accuracy, and (d) non-compression, i.e. that it does not tend to *square off* a smooth solution.

The TVD diagrams of Sweby[11] and the normalized variable formulation (NVF) methodology of Leonard[12] provide a conceptual framework for the development and analysis of high-resolution convection–diffusion schemes. The SMART,[13] SHARP[14] and UMIST[15] schemes are monotonic implementations of Leonard's third-order QUICK[1] scheme. These formulations switch between QUICK and lower-order schemes depending upon the local value of the ratio of gradients used to identify the presence of an extremum. Darwish and Moukalled[16] developed a new normalized variable and space formulation (NVSF) in which spatial parameters are introduced so as to extend the applicability of the NVF methodology to non-uniformly discretized orthogonal domains.

However, most flux limiters have been developed for schemes for uniform meshes or at most non-uniform orthogonal meshes. They can only be used for non-orthogonal meshes if the domain is transformed onto an orthogonal one. Recently Verma and Eswaran[2] developed an overlapping control volume (OCV) scheme to solve steady state 2D convection–diffusion problems directly (without transformation) on non-orthogonal structured meshes. The method was shown to be second-order-accurate and to have good convergence properties. Verma *et al.*[17] extended this scheme to time-dependent convection-diffusion problems.

In this study we attempt to develop a flux-limiting scheme for the OCV method which can be applied directly on non-orthogonal grids in the physical domain and which is simple to implement and yet approximately retains the accuracy of the base scheme.

2. FORMULATION

The details of the OCV formulation are given elsewhere,[2] but for the sake of completeness we give a brief description here. The solution domain is discretized into a structured non-orthogonal grid as shown in Figure 1(a). A typical control volume is shown by the shaded area in the figure and also in Figure 1(b). It can be seen that each interior grid point has a control volume associated with it, of which it is the central node. Hence, we can refer to these control volumes by the index of this central node, e.g. the control volume for (i, j) is shown in Figure 1(b). It can be seen that adjacent control volumes will overlap to some extent.

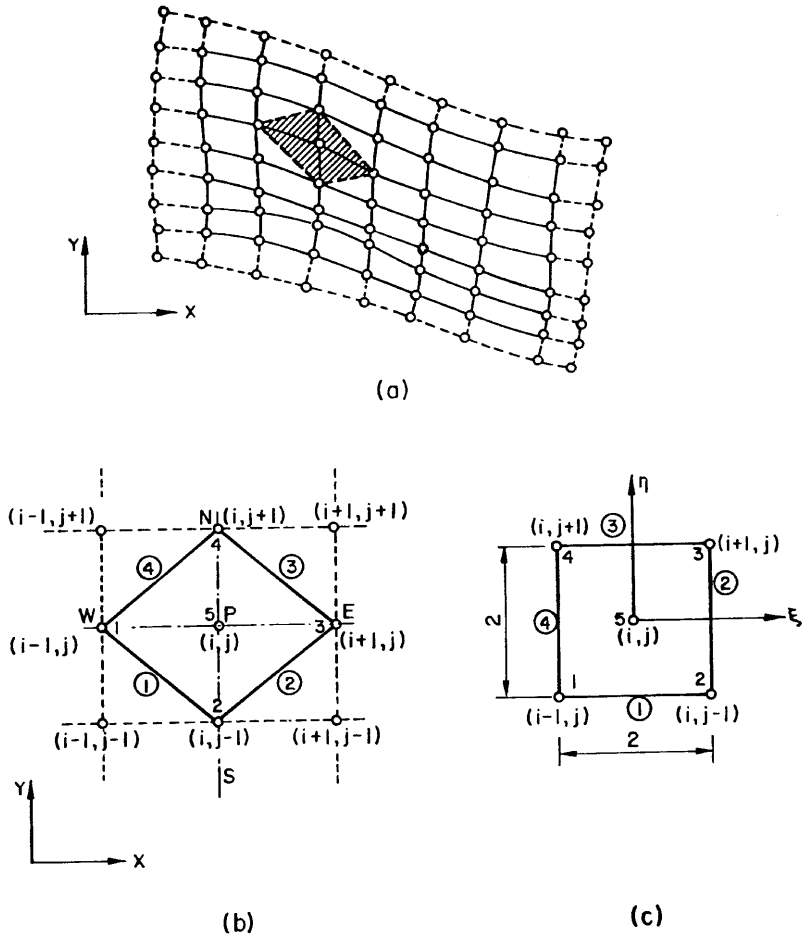

Figure 1. (a) Discretization of solution domain. (b) Control volume corresponding to shaded area in (a). (c) Mapping of control volume in (b) onto a square

2.1. *Governing equations for a control volume*

The conservation form of the two-dimensional time-dependent convection–diffusion equation for a scalar ϕ is

$$\frac{\partial(\rho\phi)}{\partial t} + \nabla \cdot (\rho \tilde{U}\phi) = \nabla \cdot (\Gamma \nabla \phi) + S_\phi, \tag{1}$$

where ρ is the density, $\tilde{U}$ is the velocity vector having components u and v in directions x and y respectively, Γ is the diffusion coefficient and S_ϕ is a source term. On integrating equation (1) over the control volume (cv) and applying the Gauss divergence theorem, we get

$$\frac{\partial}{\partial t}\int_{\mathrm{cv}} \rho\phi \, \mathrm{d}A + \oint_{\mathrm{cs}} \phi(\rho u n_x + \rho v n_y) \, \mathrm{d}l = \oint_{\mathrm{cs}} \Gamma\left(\frac{\partial \phi}{\partial x} n_x + \frac{\partial \phi}{\partial y} n_y\right) \mathrm{d}l + \int\int S_\phi \, \mathrm{d}A, \tag{2}$$

where $\mathrm{d}l$ is an elemental length on the boundary (cs) of the control volume and n_x and n_y are the direction cosines of the outward normal $\tilde{n}$ of $\mathrm{d}l$. The contour integration is counter-clockwise.

The transient term is discretized as

$$\int_{\mathrm{cv}} \rho \frac{\partial \phi}{\partial t}\, \mathrm{d}A \approx \rho \left(\frac{\phi_{i,j}^{n+1} - \phi_{i,j}^{n}}{\Delta t} \right) A_{\mathrm{s}}, \tag{3}$$

where A_{s} is the area of the control volume and n and $n+1$ are time step indices. The other terms are evaluated at $n+1$ (for a fully implicit scheme) or at n (for an explicit scheme) or as a linear combination of the two (e.g. for Crank–Nicolson[17]). In this paper we use only the explicit scheme for the unsteady test cases.

The discretization of the convection and diffusion terms is given in detail by Verma and Eswaran.[2] The discretizations use five-point shape functions and incorporate second-order upwinding in the convective term. As the convective term discretization is critical to the exposition of this paper, we present it briefly below.

Using the midpoint rule, we approximate the convective term

$$\begin{aligned} \oint_{\mathrm{cs}} \phi(\rho u n_x + \rho v n_y)\, \mathrm{d}l &= \sum_{k=1}^{4} \phi^{(k)}(\rho u^{(k)} \Delta y^{(k)} - \rho v^{(k)} \Delta x^{(k)}) \\ &= \sum_{k=1}^{4} \phi^{(k)} F^{(k)}, \end{aligned} \tag{4}$$

where the superscript (k) refers to the edges of the control volume (shown circled in Figure 1(b)). For edge k, $k=1, 2, 3$, the approximation used is (assuming constant density ρ)

$$\begin{aligned} u^{(k)} &= 0{\cdot}5(u_k + u_{k+1}), & v^{(k)} &= 0{\cdot}5(v_k + v_{k+1}), \\ \Delta y^{(k)} &= (y_{k+1} - y_k), & \Delta x^{(k)} &= (x_{k+1} - x_k), \end{aligned}$$

where the subscript k refers to the local grid point number (shown in Figure 1(b)). For $k=4$, u_{k+1}, v_{k+1}, etc. are replaced by u_1, v_1, etc. respectively in the above equations.

The *outward* mass flux through edge k is

$$F^{(k)} = (\rho u \Delta y - \rho v \Delta x)^{(k)}. \tag{5}$$

To incorporate upwinding, $\phi^{(k)}$ in (4) is approximated at the midpoint of face k by interpolation within the *upwind* control volume, which is determined by the flow direction across the face.

Second-order upwinding. The OCV scheme[2] uses second-order upwinding for the convective term. In this case, if $F^{(1)}$ is negative (i.e. flow is entering the control volume across face 1), then $\phi^{(1)}$ is approximated by interpolation within control volume $(i-1, j-1)$. That is, the values at the grid points constituting control volume $(i-1, j-1)$, through which the flow enters control volume (i, j), are used for the interpolation of $\phi^{(1)}$ at the centre of face 1. Otherwise, if $F^{(1)}$ is positive, the values at the grid points of control volume (i, j) are used to interpolate $\phi^{(1)}$ at face 1.

First-order upwinding. We can get a first-order estimate $\phi_1^{(k)}$ by simply equating the face value to the value at the central node of the upwind cell. For example, if $F^{(1)}$ is negative, then $\phi^{(1)}$ is approximated by $\phi_{i-1,j-1}$, or if $F^{(1)}$ is positive, by the value $\phi_{i,j}$.

Both these upwinding schemes for convective modelling are conservative. The method used for interpolation in the second-order upwinding is based on finite-element-type shape functions and is explained below.

2.2. Interpolation

Control volume (i, j) is mapped onto a square in (ξ, η)-space as shown in Figure 1(c), with node (i, j) at $(0, 0)$ and the other nodes at the vertices $(\pm 1, \pm 1)$ respectively. The following shape functions are used for the interpolations,

$$\begin{aligned} N_1 &= 0{\cdot}25(-\xi - \eta - \xi\eta) + 0{\cdot}125(\xi^2 + \eta^2), \\ N_2 &= 0{\cdot}25(\xi - \eta - \xi\eta) + 0{\cdot}125(\xi^2 + \eta^2), \\ N_3 &= 0{\cdot}25(\xi + \eta + \xi\eta) + 0{\cdot}125(\xi^2 + \eta^2), \\ N_4 &= 0{\cdot}25(-\xi + \eta - \xi\eta) + 0{\cdot}125(\xi^2 + \eta^2), \\ N_5 &= 1 - 0{\cdot}5(\xi^2 + \eta^2). \end{aligned} \tag{6}$$

The isoparametric formulation is used and the dependent variable ϕ and co-ordinates x and y in the control volume are represented as

$$\phi = \sum_{i=1}^{5} N_i \phi_i, \tag{7}$$

$$x = \sum_{i=1}^{5} N_i x_i, \tag{8}$$

$$y = \sum_{i=1}^{5} N_i y_i, \tag{9}$$

where the x_i and y_i are the x- and y-co-ordinates of the five grid points respectively. Equations (8) and (9) form the inverse map of control volume (i, j) from (ξ, η)- to (x, y)-co-ordinates.

For the purposes of (second-order) upwinding, $\phi^{(k)}$ is found by using (7) to interpolate the value at the midpoint of face k in the transformed control volume. For example, for face 1 we compute $N_1, N_2, \ldots, N_5$ at $\xi = 0, \eta = -1$ and then use equation (7).

2.3. Boundary conditions

Dirichlet boundary conditions can be implemented easily. For the control volumes next to the boundary, second-order upwinding may require one extra (fictitious) grid point outside the physical domain. The need for this fictitious point can be avoided by using first-order upwinding for these cell faces. For Neumann boundary conditions, backward or forward differencing can be used depending upon the boundary.

2.4. Solution procedure

The solution procedure for steady state and time-dependent convection–diffusion equations are described by Verma and Eswaran[2] and Verma *et al.*[17] respectively. Here the explicit scheme is used for the unsteady test cases and Gauss–Seidel iterations are used for the steady state test cases.

3. FLUX LIMITER

In common with second-order schemes, OCV displays dispersion errors. Near sharp gradients the numerical solution has unphysical overshoots and undershoots. To control these oscillations, we propose the FLOCV (flux-limited overlapping control volume) scheme, which uses a flux-limiting procedure during every iteration of the Gauss–Seidel routine or at each time step of the explicit scheme.

The algorithm that follows was partly inspired by Leonard's[12] normalized variable method. The idea, roughly, is to use second-order upwinding as much as possible, to ensure good accuracy, and lapse to first-order upwinding only for *abnormal* cells, where the use of second-order upwinding might cause unboundedness. The degree of abnormality of a cell is determined using a simple criterion, i.e. by determining whether the scalar value at the centre node of an upwind cell is outside the range of values of the cell corners. It was found that too violent a switching between first- and second-order upwinding led to problems in convergence, so a smooth transition between the two was incorporated using a parameter Δ (see below).

As mentioned above, the scalar face value $\phi^{(k)}$ in (4) can be estimated by either the second-order upwind estimate $\phi_2^{(k)}$ or the first-order one $\phi_1^{(k)}$. $\phi_2^{(k)}$ and $\phi_1^{(k)}$ are used in the flux-limiting procedure. The magnitude of the overshoots and undershoots in the solution can be controlled by using proper blending of the second-order scheme (OCV) and the first-order scheme. The blending is controlled by Δ, a switching parameter. The implementation of FLOCV is straightforward for explicit schemes, but for steady state problems or implicit schemes with iterative procedures we prefer to use a deferred correction approach similar to Khosla and Rubin.[18] In this approach the quantity $\phi^{(k)}$ in the middle of the cell face is approximated as

$$[\phi^{(k)}]^{n+1} = [\phi^{(k)} - \phi_1^{(k)}]^n + [\phi_1^{(k)}]^{n+1}, \tag{10}$$

where n and k are the interation index and face number respectively. For an explicit scheme, $\phi^{(k)}$ is computed only once per time step and is used directly.

The interpolated value $\phi^{(k)}$ is limited by the following procedure to control oscillations.

For each control volume (i, j) we define

$$\phi_{\min} = \min(\phi_{i-1,j}, \phi_{i+1,j}, \phi_{i,j+1}, \phi_{i,j-1}), \tag{11}$$

$$\phi_{\max} = \max(\phi_{i-1,j}, \phi_{i+1,j}, \phi_{i,j+1}, \phi_{i,j-1} \tag{12}$$

and the normalized values

$$\tilde{\phi}_c = \frac{\phi_{i,j} - \phi_{\min}}{\phi_{\max} - \phi_{\min}}, \tag{13}$$

$$\tilde{\phi}_2^{(k)} = \frac{\phi_2^{(k)} - \phi_{\min}}{\phi_{\max} - \phi_{\min}} \tag{14}$$

$$\tilde{\phi}_1^{(k)} = \frac{\phi_1^{(k)} - \phi_{\min}}{\phi_{\max} - \phi_{\min}}. \tag{15}$$

For each *outflow* face (i.e. any face for which (i, j) is the upwind cell) the normalized scalar value of the face, $\phi^{(\tilde{k})}$, is chosen by the following algorithm:

$$\begin{aligned}
&\text{if } \tilde{\phi}_c \leqslant 0, \quad \text{then } \tilde{\phi}^{(k)} = \tilde{\phi}_1^{(k)},\\
&\text{else if } 0 \leqslant \tilde{\phi}_c \leqslant \Delta, \quad \text{then } \tilde{\phi}^{(k)} = \left(\frac{\Delta - \tilde{\phi}_c}{\Delta}\right)\tilde{\phi}_1^{(k)} + \left(\frac{\tilde{\phi}_c}{\Delta}\right)\tilde{\phi}_2^{(k)},\\
&\text{else if } \Delta \leqslant \tilde{\phi}_c \leqslant 1 - \Delta, \quad \text{then } \tilde{\phi}^{(k)} = \tilde{\phi}_2^{(k)},\\
&\text{else if } 1 - \Delta \leqslant \tilde{\phi}_c \leqslant 1, \quad \text{then } \tilde{\phi}^{(k)} = \left(\frac{\tilde{\phi}_c + \Delta - 1}{\Delta}\right)\tilde{\phi}_1^{(k)} + \left(\frac{1 - \tilde{\phi}_c}{\Delta}\right)\tilde{\phi}_2^{(k)},\\
&\text{if } \tilde{\phi}_c > 1, \quad \text{then } \tilde{\phi}^{(k)} = \tilde{\phi}_1^{(k)}.
\end{aligned}$$

This algorithm simply chooses the face value $\tilde{\phi}^{(k)}$ to be $\tilde{\phi}_1^{(k)}$ if $\tilde{\phi}_c > 1$ or $\phi_c < 0$, $\phi_2^{(k)}$ if $\Delta \leqslant \tilde{\phi}_c \leqslant 1 - \lambda, \Delta$, or else takes a weighted average of the first- and second-order estimates. The value of Δ obviously has to be less than 0·5. The unnormalized value of $\phi^{(k)}$ can be recovered from the normalized value by

$$\phi^{(k)} = \tilde{\phi}^{(k)}(\phi_{\max} - \phi_{\min}) + \phi_{\min}.$$

The sensitivity of FLOCV to the switching parameter Δ is analysed below for test cases with discontinuities as well as smooth gradients and extrema. Smaller values of Δ are preferable for *smooth* solutions, because this means that the scheme will rarely use first-order upwinding. However, in the presence of shock-like discontinuities, large Δ-values are more likely to yield bounded solutions. Thus the value of Δ should be chosen optimally to trade off the opposing requirements of accuracy and boundedness. While we cannot expect a given value of Δ to be universally optimum in all situations, our experience has led us to conclude that $\Delta \equiv 0{\cdot}2$–$0{\cdot}3$ would generally work well. The details of the numerical experiments are given in the next section.

4. RESULTS

Three steady state and two time-dependent pure convection problems are solved here and the efficacy of FLOCV in controlling non-physical oscillations near the regions of steep gradient is tested. In all cases the governing equation is (1) or its steady state counterpart with $\Gamma = 0$. The simple explicit temporal scheme is used to solve the time-dependent convection problems (Test problems 3 and 4).

The performance evaluation is based on the following parameters: (i) the maximum field value, (ii) the minimum field value and (iii) the RMS error. The predicted maximum and minimum values show the effectiveness of the scheme in preserving boundedness, while the RMS error is a measure of the overall performance of the scheme. The RMS error is defined as

$$\mathrm{RMS} = \left(\frac{\sum_{N_{\text{total}}} (\phi^{\text{NUMERICAL}} - \phi^{\text{EXACT}})^2}{N_{\text{total}}} \right)^{1/2}, \tag{16}$$

where N_{total} denotes the total number of interior grid points.

4.1. Test problem 1

This model problem, first proposed by Raithby,[19] is widely used to test the cross-stream numerical diffusion of difference schemes.

The problem is shown in Figure 2(a). The flow is assumed uniform through the square domain, making an angle such that the streamline through $(0, y_c)$ passes through the centre of the square. The scalar field at the left (inflow) boundary has an abrupt step change, with ϕ=1 above y_c and $\phi = 0$ below. The Peclet number is taken as infinity ($\Gamma = 0$) and thus the scalar is transported by convection only. The boundary conditions are shown on the figure. The value of ϕ is fixed so as to be 0·5 at the point of the step change, $y = y_c, x = 0$. The exact solution for this problem is the advection of the step change in the flow direction without any diffusion, i.e. $\phi = 1$ above the slanted line shown and $\phi = 0$ below it.

A regular 21×21 grid is used to discretize the solution domain. The other input parameters are $\Gamma = 0$ and the various flow angles corresponding to $y_c = 0$, 1, 2, 3, 4 and 5. The sensitivity of FLOCV to the switching parameter Δ is studied and the results are presented in Tables I–IV in tabular form for different values of Δ at different flow angles. The RMS error along the *midplane* ($x = 5$) and the *global* maximum and minimum values of ϕ are shown in Tables I and II. It can be observed that as Δ

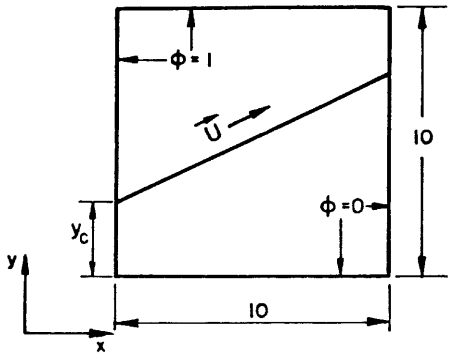

Figure 2(a). Schematic diagram of Test problem 1

increases, (a) the RMS errors decrease and then increase and (b) the levels of undershoots and overshoots decrease. The initial decrease in RMS error is due to the removal of under/overshoots and the RMS error then increases owing to the fall in accuracy as Δ approaches 0·5. The optimum choice of Δ seems to be between 0·2 and 0·3 (this conclusion is reinforced by other results below).

A comparison of FLOCV with other schemes is also presented. The results at the midplane ($x = 5$) are shown in Figures 2(b)–2(g) for different flow angles. The results for the conventional upwind scheme, OCV and FLOCV (with $\Delta = 0{\cdot}3$) are shown in the figures. As expected, the conventional upwind scheme does not show any overshoots or undershoots, gives the exact solution when the flow is aligned with the grid lines ($Y_c = 5$), but is highly diffusive when the flow is oblique to the grid lines. The unbounded OCV scheme shows overshoots and undershoots near the sharp gradient. It can be seen that FLOCV removes the oscillations associated with the unbounded OCV scheme quite effectively when Δ is chosen as 0·3.

The effect of grid irregularity on the solution accuracy of FLOCV is demonstrated by solving the above problem on a distorted grid. The interior grid points are randomly perturbed from their original

Table I. Sensitivity of FLOCV to switching parameter Δ for Test problem 1

	$Y_c = 0$			$Y_c = 1$			$Y_c = 2$		
Δ	Max.	Min.	RMS	Max.	Min.	RMS	Max.	Min.	RMS
0·1	1·0	0·0	$3{\cdot}528 \times 10^{-5}$	1·0	$-3{\cdot}822 \times 10^{-2}$	0·054	1·0	$-3{\cdot}822 \times 10^{-2}$	0·0700
0·2	1·0	0·0	$5{\cdot}954 \times 10^{-5}$	1·0	$-2{\cdot}276 \times 10^{-2}$	0·0495	1.0	$-2{\cdot}045 \times 10^{-2}$	0·0691
0·3	1·0	0·0	$6{\cdot}734 \times 10^{-5}$	1·0	$-1{\cdot}484 \times 10^{-3}$	0·0527	1·0	$-1{\cdot}794 \times 10^{-8}$	0·0654
0·4	1·0	0·0	$5{\cdot}596 \times 10^{-5}$	1·0	0·0	0·0605	1·0	0·0	0·0732

Table II. Sensitivity of FLOCV to switching parameter Δ for Test problem 1

	$Y_c = 3$			$Y_c = 4$			$Y_c = 5$		
Δ	Max.	Min.	RMS	Max.	Min.	RMS	Max.	Min.	RMS
0·1	1·00005	$-3{\cdot}091 \times 10^{-2}$	0·0751	1·006	$-2{\cdot}213 \times 10^{-2}$	0·0763	1·0093	$-9{\cdot}226 \times 10^{-3}$	0·0756
0·2	1·0	$-9{\cdot}797 \times 10^{-3}$	0·0731	1·0	$-7{\cdot}405 \times 10^{-6}$	0·0750	1·0	0·0	0·0753
0·3	1·0	0·0	0·0714	1·0	0·0	0·0724	1·0	0·0	0·0725
0·4	1·0	0·0	0·0793	1·0	0·0	0·0813	1·0	0·0	0·0844

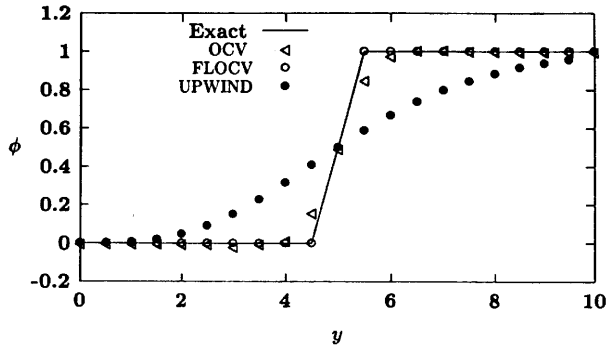

Figure 2(b). Results for Test problem 1, $y_c = 0$

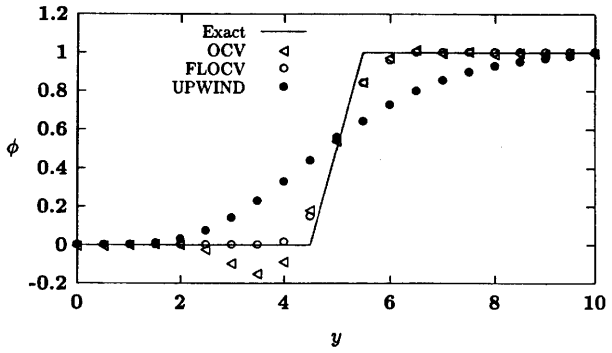

Figure 2(c). Results for Test problem 1, $y_c = 1$

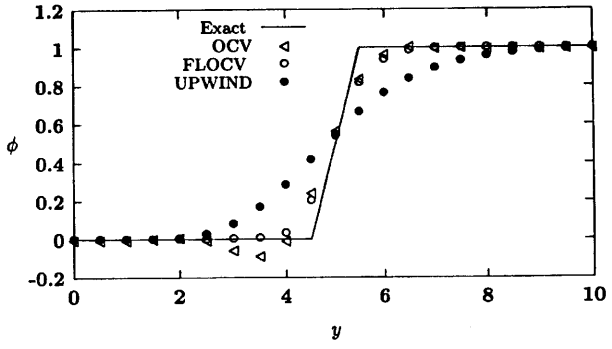

Figure 2(d). Results for Test problem 1, $y_c = 2$

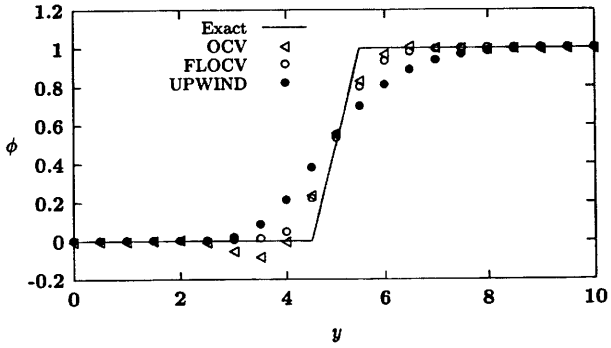

Figure 2(e). Results for Test problem 1, $y_c = 3$

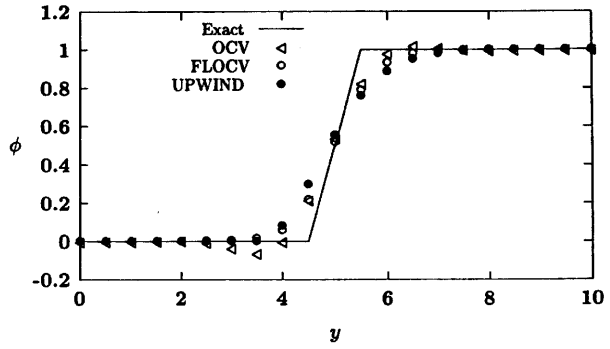

Figure 2(f). Results for Test problem 1, $y_c = 4$

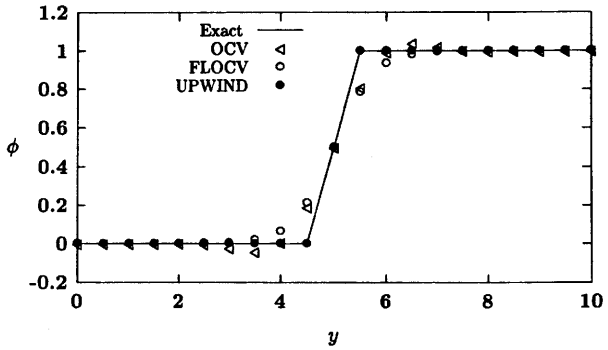

Figure 2(g). Results for Test problem 1, $y_c = 5$

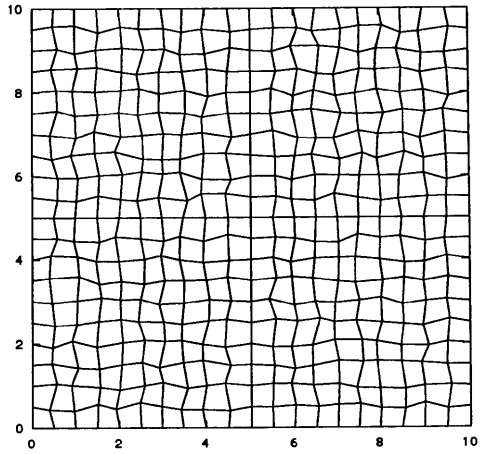

Figure 2(h). Distorted (20%) grid

uniform positions by 5%, 10% and 20% of the average grid distance (i.e. each interior grid point is shifted from the uniform grid position by Δx_s and Δy_s in the x- and y-direction, where Δx_s and Δy_s are uniformly distributed random numbers lying between $\pm(\%\text{distortion}) \times \Delta x/100$ and $\pm(\%\text{distortion}) \times \Delta y/100$ respectively. A typical grid lay-out with 20% distortion is shown in Figure 2(h). The results are presented in Tables III and IV for two grid levels of 21×21 and 41×41 at a flow angle corresponding to $Y_c = 3$.

The results show that while the RMS errors do increase with increasing grid distortion, the overshoots and undershoots are effectively contained by FLOCV with $\Delta = 0{\cdot}3$ (at the expense of a slight degradation of accuracy).

4.2. *Test problem 2*

The computational domain is shown in Figure 3(a). The velocity components are $u = y$ and $v = -x$. Again the problem is a purely convective one ($\Gamma = 0$), so any scalar profile specified along OA in Figure 3(a) should be swept unchanged along the streamlines and reproduced unchanged at OB, OC and OD (after going through a 90°, 180° and 270° turn respectively). A scalar profile used by Smith and Hutton[20] is specified along OA:

$$\phi = 1 + \tanh[10(2x + 1)], \quad y = 0, -1 \leqslant x \leqslant 0.$$

Table III. Effect of grid distortion on performance of OCV for Test problem 1 corresponding to $Y_c = 3$

Distortion (%)	Grid 21×21			Grid 41×41		
	Max.	Min.	RMS	Max.	Min.	RMS
0	1·01750	−0·13531	0·07205	1·01749	−0·15320	0·06440
5	1·02516	−0·13125	0·07267	1·01644	−0·15039	0·06516
10	1·03280	−0·12669	0·07350	1·01800	−0·14684	0·06585
20	1·05102	−0·11633	0·07571	1·02063	−0·13746	0·06702

Table IV. Effect of grid distortion on performance of FLOCV with $\Delta = 3$ for Test problem 1 corresponding to $Y_c = 3$

Distortion (%)	Grid 21×21			Grid 41×41		
	Max.	Min.	RMS	Max.	Min.	RMS
0	1·0	0·0	0·07144	1·0	0·0	0·05958
5	1·0	0·0	0·07275	1·0	0·0	0·06023
10	1·0	0·0	0·07450	1·0	0·0	0·06260
20	1·0	0·0	0·07861	1·0	0·0	0·07005

The boundary condition is given by

$$\phi = 0, \quad \begin{cases} x = -1, -1 \leqslant y \leqslant 1, \\ y = -1, -1 \leqslant x \leqslant 1, \\ y = 1, -1 \leqslant x \leqslant 1, \\ x = 1, -1 \leqslant y \leqslant 1. \end{cases}$$

Two numerical solutions are obtained using 41×41 and 81×81 grid points respectively. The computed profiles after 90°, 180° and 270° rotations are shown in Figures 3(b)–3(g) for the conventional upwind, OCV and FLOCV ($\Delta = 0{\cdot}3$) schemes. The results for the conventional upwind scheme are very diffusive and the magnitude of numerical diffusion increases as the angle of rotation increases. It can be seen in Figures 3(b)–3(d) that OCV allows small overshoots and undershoots; however, these reduce in magnitude as the mesh is refined, as shown in Figures 3(e)–3(g). When FLOCV is used, it removes the overshoots and undershoots (Figures 3(b)–3(d)) while introducing very little numerical diffusion. The results for the refined mesh, shown in Figures 3(e)–3(g), are in close agreement with the exact solution.

This test problem is also solved on distorted grids. The overshoots and undershoots are shown in Table V to be effectively contained by FLOCV. The level of RMS error for distortion up to 5% is approximately the same as that on a uniform grid.

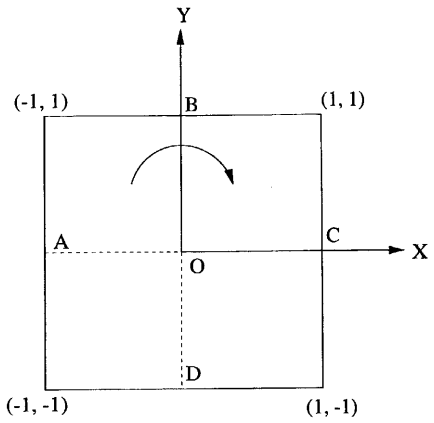

Figure 3(a). Schematic diagram of Test problem 2

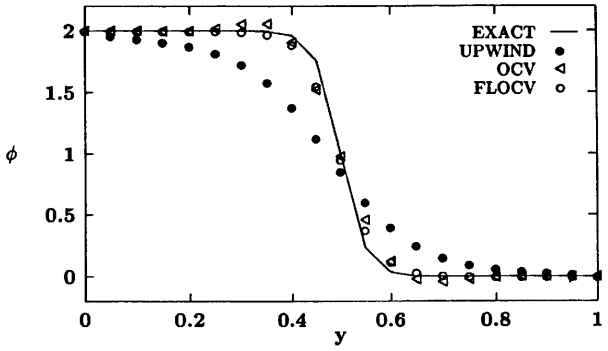

Figure 3(b). Results for Test problem 2 along OB (grid 41×41)

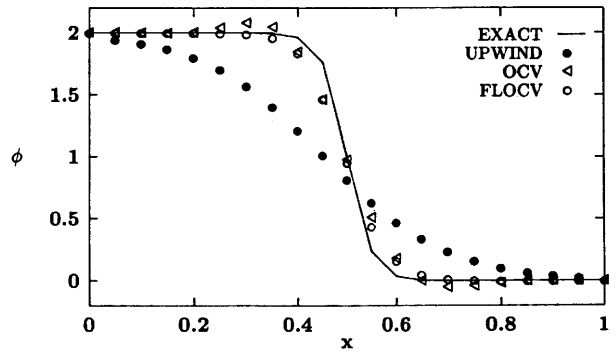

Figure 3(c). Results for Test problem 2 along OC (grid 41×41)

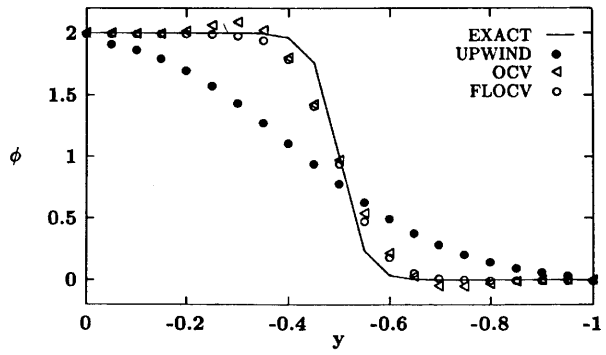

Figure 3(d). Results for Test problem 2 along OD (grid 41×41)

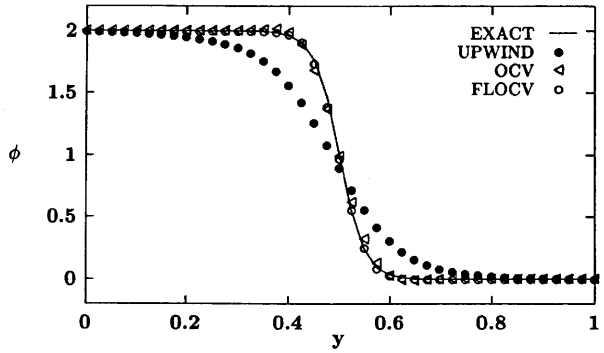

Figure 3(e). Results for Test problem 2 along OB (grid 81×81)

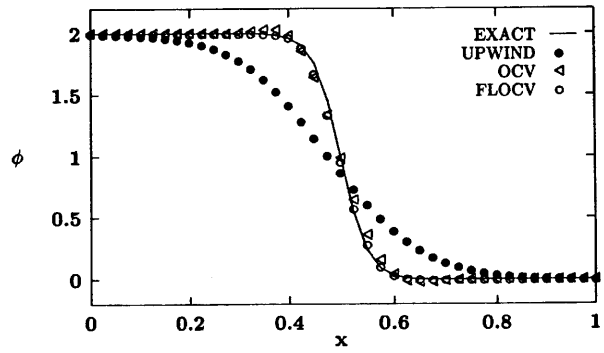

Figure 3(f). Results for Test problem 2 along OC (grid 81×81)

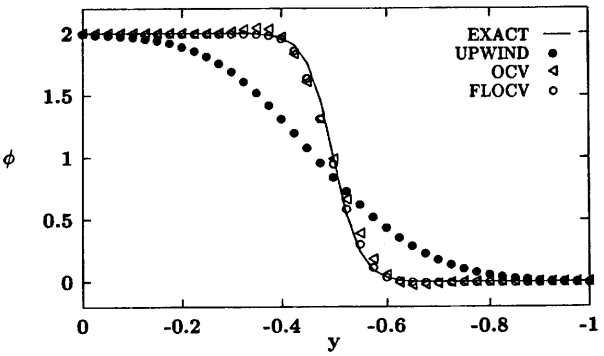

Figure 3(g). Results for Test problem 2 along OD (grid 81×81)

Table V. Effect of grid distortion on performance of FLOCV with $\Delta = 0{\cdot}3$ for Test problem 2

Distortion (%)	Grid 41×41			Grid 81×81		
	Max.	Min.	RMS (along OD)	Max.	Min.	RMS (along OD)
0	1·99999	0·0	0·11233	1·99999	0·0	0·03263
5	2·00048	0·0	0·11417	2·00016	0·0	0·03469
10	2·00084	0·0	0·13503	2·00031	0·0	0·04227
20	2·00162	$-2{\cdot}3 \times 10^{-10}$	0·185302	2·00056	0·0	0·09376

4.3. Test problem 3

This problem is that of an advancing front in a unidirectional flow and is included to demonstrate the capability of the proposed flux limiter in removing overshoots and undershoots in unsteady computations.

A schematic diagram of the problem is shown in Figure 4(a). A step input is specified at the inlet. The boundary conditions at the other boundaries are homogeneous Neumann conditions. The velocity components u and v are 0·5 and 0·0 respectively. The diffusion coefficient Γ is zero, i.e. the flow is purely convective. Therefore any profile specified at the inlet is advected downstream without any change and can be used as an exact solution at the front position at any point in time. The computational domain is divided into 65×65 uniform meshes. Two different time steps, $\Delta t = 48$ and 96 units, corresponding to Courant numbers ($\equiv u\Delta t/\Delta x$) of 0·12 and 0·24 respectively, are used in the computations. The results are shown (for $t = 9600$) in Figures 4(b) and 4(c) for OCV and FLOCV along with the exact solution. It can be seen that the oscillations are removed by FLOCV. The performance of the flux limiter along with the base scheme can also be judged on the basis of the three parameters E_w, the total variation of errors or the waviness, E_t, the total absolute error, and E_s, the spreading index, as defined below:

$$E_w = \sum_{i=1}^{i_{max}} |e_{i+1} - e_i|, \tag{17}$$

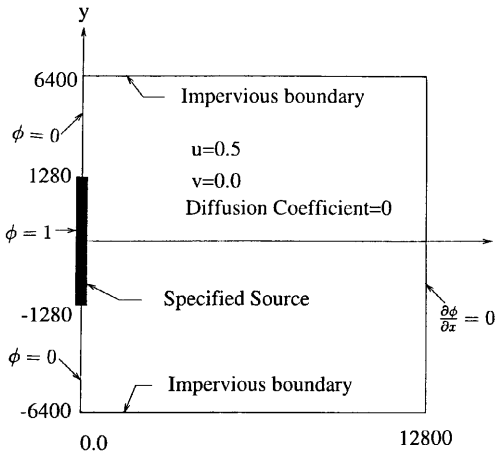

Figure 4(a). Schematic diagram of Test problem 3

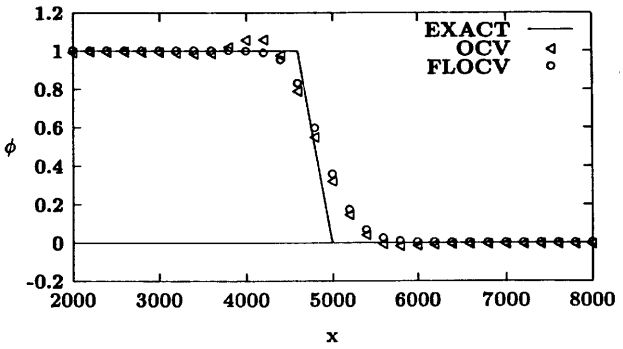

Figure 4(b). Results for Test problem 3 ($\Delta t = 48$)

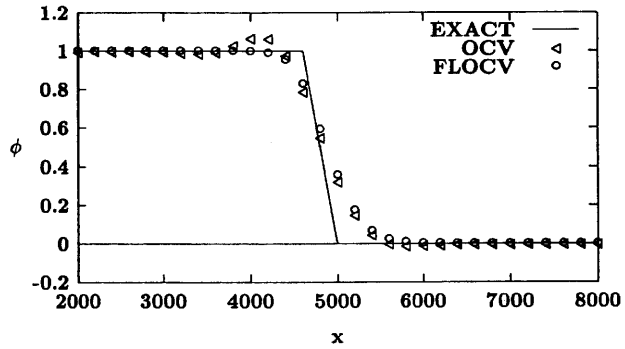

Figure 4(c). Results for Test problem 3 ($\Delta t = 96$)

where e_i is the error in the solution and at grid point i (at $j = j_{\text{mid}}$ corresponding to the centreline $y = 0$);

$$E_{\text{t}} = \sum_{i=1}^{i_{\max}} \Delta x_i |e_i|; \tag{18}$$

$$E_{\text{s}} = \sum_{i=1}^{i_{\max}} \Delta x_i |x_i - x_{\text{f}}||e_i|, \tag{19}$$

where x_{f} is the position of the front at the given time.

The performance parameters are presented in Tables VI–VIII for the OCV and FLOCV schemes. The flux limiter considerably improves the performance of the original scheme. It smoothens the waviness in the solution, reduces the total absolute error and decreases the numerical spreading.

Table VI. Test problem 3—total variation of errors or waviness (E_{w})

Δt	OCV	FLOCV
48	1·75	1·52
96	1·76	1·52

Table VII. Test problem 3—total absolute error (E_t)

Δt	OCV	FLOCV
48	281·46	252·95
96	286·64	254·24

Table VIII. Test problem 3—spreading index (E_s)

Δt	OCV	FLOCV
48	$8{\cdot}76 \times 10^4$	$5{\cdot}49 \times 10^4$
96	$9{\cdot}08 \times 10^4$	$5{\cdot}53 \times 10^4$

4.4. Test problem 4

In this test case a square-shaped scalar field is advected. A schematic diagram of the problem is shown in Figure 5(a). The source field (shaded) has a scalar value of 10 and the rest of the domain has a scalar value of zero. The scalar field was initially centred at the point $(-1{\cdot}5, -1{\cdot}5)$ and advected by a uniform velocity field, making 45° with the co-ordinate lines, to the position (1·5, 1·5). The velocity components u and v are of unit magnitude.

This test is very stringent, as many lines of discontinuities exist in the problem. The *global* RMS error and minimum and maximum of the computed scalar field for OCV and FLOCV are presented, for two grids of 41×41 and 81×81 grid points, in Table IX for a Courant number of 0·20. It can be seen that the flux limiter works satisfactorily and considerably improves the results. Tamamidis and Assanis[21] have compared the performance of various schemes for this problem. These results are shown in Table X. It is clear that the performance of FLOCV is comparable with that of MPL,[22] MSOU[23] and SHARP.[14] The perspective plots of the scalar field are shown in Figures 5(b)–5(d) for the OCV and FLOCV results for grids of 81×81. The initial scalar field is shown in Figure 5(b) and the final fields are shown in Figures 5(c) and 5(d) for OCV and FLOCV respectively. It can be seen that the flux limiter works well and considerably improves the solution.

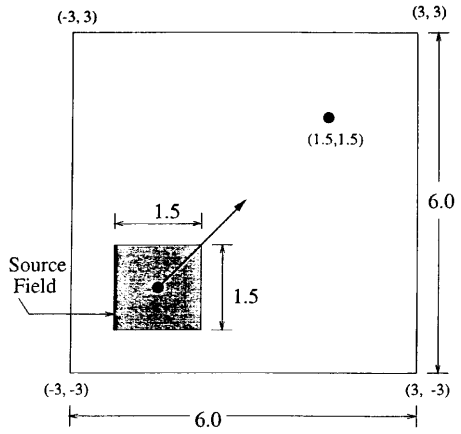

Figure 5(a). Schematic diagram of Test problem 4

Table IX. Results for Test problem 4—Courant number 0·20

	Grid 41×41			Grid 81×81		
Scheme	Max.	Min.	RMS	Max.	Min.	RMS
OCV	23·164	−7·658	1·999	41·006	−26·727	4·173
FLOCV	9·992	0·0	0·755	10·0	0·0	0·5312

Table X. Results for Test problem 4—results reported by Tamamidis and Assanis[21]

	Grid 40×40			Grid 80×80		
Scheme	Max.	Min.	RMS	Max.	Min.	RMS
FOU	6·257	0·0	1·445	8·526	0·0	1·289
SOU	16·356	−3·58	1·268	18·880	−5·575	1·329
QUICK	18·808	−5·88	1·737	35·471	−21·092	3·366
MPL	9·973	0·0	0·936	10·0	0·0	0·717
MSOU	10·0	0·0	0·855	10·0	0·0	0·537
SHARP	10·219	−0·44	0·948	10·892	−1·373	0·652

4.5. Test problem 5

This test was used to show the efficacy of the convection modelling of the OCV method by Verma and Eswaran.[2] This test case computes a smooth solution and is selected to demonstrate the effect of flux limiting on the order of accuracy and to show how diffusive and/or overcompressive FLOCV might be. The computational domain and boundary conditions are the same as shown in Figure 3(a). The velocity components are defined as $u = y$ and $v = -x$. Again the problem is purely convective ($\Gamma = 0$), so any scalar profile specified along OA in Figure 3(a) should be reproduced unchanged at

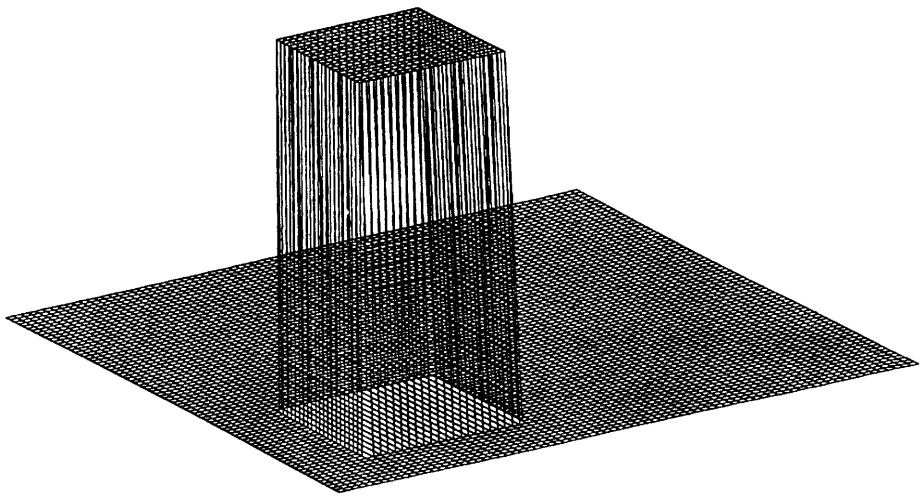

Figure 5(b). 3D perspective plot of initial scalar field for Test problem 4

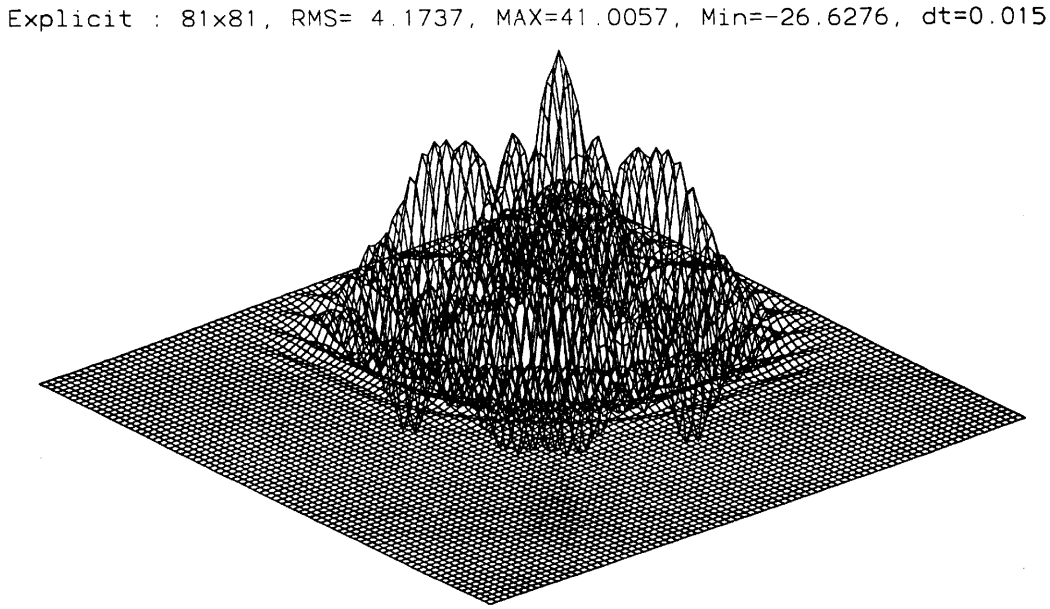

Figure 5(c). 3D perspective plot of scalar field predicted by OCV scheme

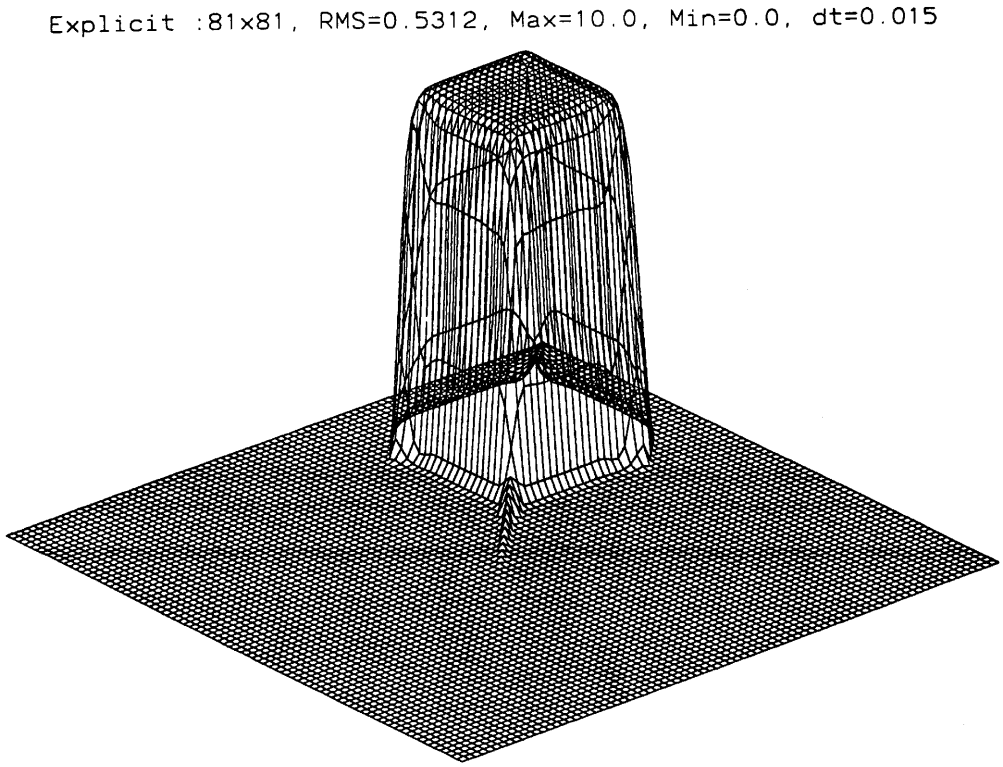

Figure 5(d). 3D perspectibve plot of scalar field predicted by OCV with FLOCV

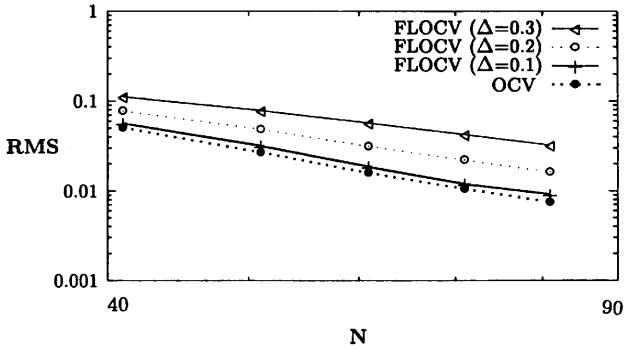

Figure 6(a). RMS error versus N for Test problem 5 (along OD) on uniform grid

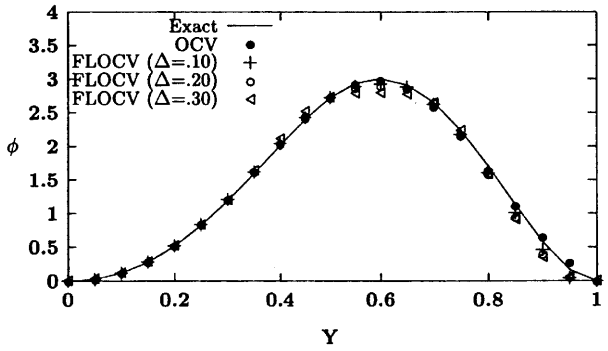

Figure 6(b). Computed profile along OD on 41×41 grid

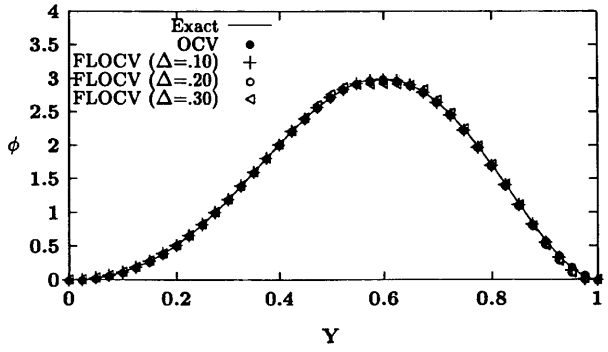

Figure 6(c). Computed profile along OD on 81×81 grid

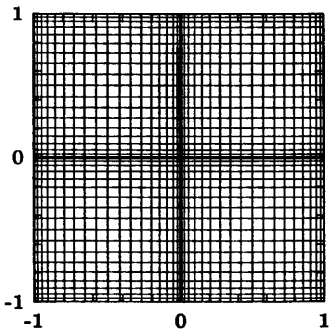

Figure 6(d). Non-uniform Cartesian grid

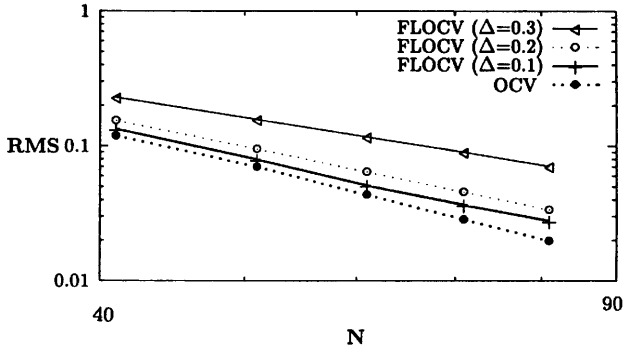

Figure 6(e). RMS error versus N for Test problem 5 (along OD) on non-uniform grid

OD (after going through a 270° turn). The profile specified along OA is the smooth Gaussian distribution $\phi = e^{2|x|} \sin^2(\pi x)$.

The computational domain is discretized using $N \times N$ uniform grids with $N = 41$, 51, 61, 71 and 81. The RMS errors of the points on OD (*not* for the entire domain) for OCV and FLOCV with different values of Δ at various grid levels are shown in Figure 6(a) on a log–log scale. If the error ε is assumed proportional to Δx^m, where m is the order of the method, then the values of m are 2·7481, 2·6327, 2·2547 and 1·7788 for OCV and FLOCV with $\Delta = 0{\cdot}1$, 0·2 and 0·3 respectively. It can be seen that FLOCV maintains second-order accuracy up to $\Delta = 0{\cdot}2$ and there is only a small deterioration for $\Delta = 0{\cdot}3$.

The computed ϕ-profiles along OD at grid levels of 41×41 and 81×81 are shown in Figures 6(b) and 6(c) respectively for different values of Δ. It can be observed that FLOCV is slightly compressive

Table XI. Test problem 5—RMS error along OD on 0% distorted grids

Grid	OCV	FLOCV ($\Delta = 0{\cdot}1$)	FLOCV ($\Delta = 0{\cdot}2$)	FLOCV ($\Delta = 0{\cdot}3$)
41×41	0·05019	0·05692	0·07760	0·11221
51×51	0·02657	0·03154	0·04825	0·07899
61×61	0·01585	0·01858	0·03141	0·05711
71×71	0·01048	0·01190	0·02199	0·04195
81×81	0·00747	0·00917	0·01626	0·03178

Table XII. Test problem 5—RMS error along OD on 5% distorted grids

Grid	OCV	FLOCV ($\Delta = 0{\cdot}1$)	FLOCV ($\Delta = 0{\cdot}2$)	FLOCV ($\Delta = 0{\cdot}3$)
41×41	0·05111	0·06002	0·07986	0·11509
51×51	0·02669	0·03214	0·04911	0·07944
61×61	0·01844	0·02101	0·03368	0·05938
71×71	0·01168	0·01339	0·02400	0·04349
81×81	0·00855	0·00995	0·01682	0·03288

Table XIII. Test problem 5—RMS error along OD on 10% distorted grids

Grid	OCV	FLOCV ($\Delta = 0{\cdot}1$)	FLOCV ($\Delta = 0{\cdot}2$)	FLOCV ($\Delta = 0{\cdot}3$)
41×41	0·05443	0·06488	0·08592	0·11868
51×51	0·02933	0·03619	0·05306	0·08163
61×61	0·02275	0·02687	0·03940	0·06421
71×71	0·01406	0·01656	0·02782	0·04667
81×81	0·01160	0·01275	0·01996	0·03544

Table XIV. Test problem 5—RMS error along OD on 20% distorted grids

Grid	OCV	FLOCV ($\Delta = 0{\cdot}1$)	FLOCV ($\Delta = 0{\cdot}2$)	FLOCV ($\Delta = 0{\cdot}3$)
41×41	0·06639	0·08012	0·10363	0·13141
51×51	0·03964	0·05311	0·06749	0·09256
61×61	0·03372	0·04162	0·05423	0·07391
71×71	0·02059	0·02617	0·03818	0·05331
81×81	0·01844	0·02267	0·02951	0·04088

(i.e. it tends to *square off* the solution near the peak, especially for $\Delta = 0{\cdot}3$ on the coarse mesh). However, grid refinement improves the solution considerably in Figure 6(c). On both the coarse and fine meshes, diffusive errors are small.

The solution of FLOCV for this smooth case was also obtained on the non-uniform orthogonal grid shown in Figure 6(d). (Each quadrant of this grid is a Gauss–Lobbatto Chebyshev grid of size $M \times M$,

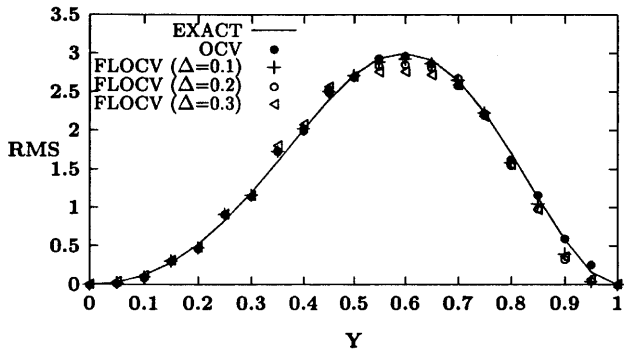

Figure 6(f). Computed profile along OD on 20% distorted grid (41×41)

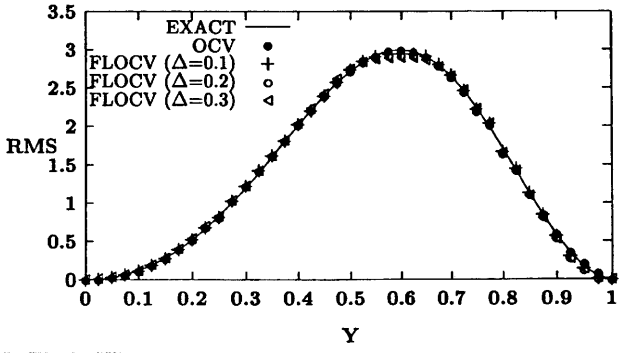

Figure 6(g). Computed profile along OD on 20% distorted grid (81×81)

resulting in a composite $N \times N$ grid with $N = 2M + 1$). A typical grid lay-out with 41×41 grid points is shown in Figure 6(d). The RMS error along OD is presented in Figure 6(e) for OCV and FLOCV (with $\Delta = 0{\cdot}1$, $0{\cdot}2$ and $0{\cdot}3$). Once again, if we assume error $\varepsilon \propto (1/N)^m$, the exponents m are 2·591, 2·270, 2·182 and 1·707 for OCV and FLOCV with $\Delta = 0{\cdot}1$, $0{\cdot}2$ and $0{\cdot}3$ respectively. It is perhaps worthy of mention that the Chebyshev grid used, while smooth, is *highly* non-uniform; for example, with $N = 81$ the ratio of the largest to the smallest grid interval is $\Delta_{\max}/\Delta_{\min} \approx 25$. It can be seen that not only is OCV second-order-accurate on this non-uniform grid, but also that FLOCV retains this order of accuracy till at least $\Delta = 0{\cdot}2$.

Next we take up the case of *non-uniform*, *non-orthogonal* grids. The grid is distorted from the uniform grid by the same means employed in Test problem 1. The effect of grid distortion on the solutions of OCV and FLOCV is shown in Table XI–XIV. The tables show the RMS errors along OD (270° turn) from the initial Gaussian profile specified at OA. It can be seen that FLOCV retains second-order accuracy up to 10% grid distortion for $\Delta \leqslant 0{\cdot}2$. The deterioration in the order of accuracy of FLOCV is not very much even on the highly (20%) distorted grid. The computed profiles along OD are also shown in Figures 6(f) and 6(g) for the 20% distorted grid.

5. CPU TIME COMPARISON AND PROGRAMMING CONSIDERATIONS

For steady state cases the steady convection–diffusion equation is solved implicitly using an approach similar to the deferred correction approach.[18] To compare the CPU time required by the OCV and FLOCV schemes, Test problem 5 is again used here. The convergence criterion selected for this problem is $|(\phi_{(i,j)}^{(k+1)} - \phi_{(i,j)}^{(k)})| < 10^{-5}$, where k is an iteration index. The results are presented in Table XV for OCV and FLOCV (with $\Delta = 0{\cdot}3$) on uniform Cartesian grids. It can be seen that the increase

Table XV. CPU time (in seconds) comparison for Test problem 5 on uniform Cartesian grids

Grid	OCV	FLOCV ($\Delta = 0{\cdot}3$)
41×41	52·137	57·288
51×51	104·692	111·764
61×61	183·088	203·998
71×71	327·558	352·860
81×81	525·349	597·575

in CPU time for FLOCV is less than 15% compared with OCV. The calculations were done on a DEC-3000 machine.

6. CONCLUSIONS

The scheme FLOCV is a flux-limited version of the base scheme OCV.[2] FLOCV switches from second- to first-order interpolation in the presence of extrema. First-order interpolation introduces numerical diffusion which damps oscillations. The switching between the different interpolation methods is controlled by a blending parameter Δ.

We have tested the performance of FLOCV under varied and arduous conditions. The cases considered in this paper include steep gradients, flow-to-grid skewness and circulating flows on uniform and non-orthogonal structured grids. FLOCV performs well in all the test cases considered. The salient results of this paper are as follows.

1. For problems with discontinuities, FLOCV is quite effective in removing oscillations associated with the unbounded OCV scheme on both orthogonal and non-orthogonal grids.
2. The effect of flux limiting on the accuracy of the base scheme was studied using a smooth Gaussian profile. It was demonstrated that FLOCV is second-order-accurate on uniform Cartesian grids for $\Delta \leqslant 0{\cdot}2$. FLOCV was also found to retain this order of accuracy even on highly non-uniform Cartesian grids. On mildly non-orthogonal grids (up to 10% distortion), FLOCV is second-order-accurate with $\Delta \leqslant 0{\cdot}2$. The deterioration in the order of accuracy of FLOCV is not much even on a 20% distorted grid.
3. FLOCV was also applied to unsteady test cases. It smoothens waviness in the solution and decreases numerical spreading as compared with the OCV scheme.
4. The performance of FLOCV was judged with other standard flux-limiting schemes in a stringent test problem (Test problem 4). FLOCV was comparable to the best of the other schemes.
5. The sensitivity of FLOCV to the switching parameter Δ was analysed. The optimum choice of Δ seems to be between 0·2 and 0·3.
6. FLOCV can be a good choice for 2D convective–diffusive problems on orthogonal and non-orthogonal structured grids.

REFERENCES

1. B. P. Leonard, 'A stable and accurate convective modelling procedure based on quadratic upstream interpolation', *Comput. Methods Appl. Mech. Eng.*, **19**, 59–98 (1979).
2. A. K. Verma and V. Eswaran, 'Overlapping control volume approach for convection–diffusion problems', *Int. j. number. methods fluids*, **23**, 865–882 (1996).
3. A. Jameson, W. Schmidt and E. Turkel, 'Numerical simulation of Euler equations by finite-volume methods using Runge–Kutta time-stepping schemes', *AIAA Paper 81-1259*, 1981.
4. J. P. Boris and D. L. Book, 'Flux-corrected transport. I: SHASTA, a fluid transport algorithm that works', *J. Comput. Phys.*, **11**, 38–69 (1973).
5. S. T. Zalesak, 'Fully multi-dimensional flux-corrected transport algorithms for fluids', *J. Comput. Phys.*, **31**, 335–362 (1979).
6. A. Harten, 'High resolution schemes for hyperbolic conservations laws', *J. Comput. Phys.*, **49**, 357–393 (1983).
7. C. W. Shu and S. Osher, 'Efficient implementation of essentially non-oscillatory shock-capturing schemes', *J. Comput. Phys.*, **77**, 439–471 (1988).
8. H. Yang, 'An artificial compression method for ENO schemes: the slope modification method', *J. Comput. Phys.*, **89**, 125–160 (1990).
9. J. C. T. Wang and G. F. Windhopf, 'A high-resolution TVD finite volume scheme for the Euler equations in conservative form', *J. Comput. Phys.*, **84**, 145–173 (1989).
10. C. Hirsch, *Numerical Computation of Internal and External Flows*, Vol. II, Wiley, New York, 1990.

11. P. K. Sweby, 'High resolution schemes using flux limiters for hyperbolic conservation laws', *SIAM J. Numer. Anal.*, **21**, 995–1001 (1984).
12. B. P. Leonard, 'Universal limiter for transient interpolation modelling of the advective transport equations: the ULTIMATE conservative difference scheme', *NASA Tech. Memo. 100916, ICOMP-88-11*, 1988.
13. P. H. Gaskel and A. K. C. Lau, 'Curvature compensated convective transport: SMART, a new boundedness preserving transport algorithm', *Int. j. numer. methods fluids*, **8**, 617–647 (1988).
14. B. P. Leonard, 'Simple high-accuracy resolution program for convective modelling of discontinuities', *Int. j. numer. methods fluids*, **8**, 1291–1318 (1988).
15. F. S. Lien and M. A. Leschziner, 'Upstream monotonic interpolation for scalar transport with application to complex turbulent flows', *Int. j. numer. methods fluids*, **19**, 527–548 (1994).
16. M. S. Darwish and F. H. Moukalled, 'Normalized variable and space formulation methodology for high resolution schemes', *Numer. Heat Transfer B*, **26**, 79–96 (1994).
17. A. K. Verma, B. Murty and V. Eswaran, 'Overlapping control volume method for solute transport problems', submitted.
18. P. K. Khosla and S. G. Rubin, 'A diagonally dominant second-order accurate implicit scheme', *Comput. Fluids*, **2**, 207–218 (1974).
19. G. D. Raithby, 'Skew upstream differencing schemes for problems involving fluid flow', *Comput. Methods Appl. Mech. Eng.*, **9**, 153–164 (1976).
20. R. M. Smith and A. G. Hutton, 'The numerical treatment of advection: a performance comparison of current methods', *Numer. Heat Transfer*, **5**, 439–461 (1982).
21. P. Tamamidis and D. N. Assanis, 'Evaluation of various high-order-accuracy schemes with and without flux limiters', *Int. j. numer. methods fluids*, **16**, 931–948 (1993).
22. V. Van Leer, 'Towards the ultimate conservative difference scheme. IV. A new approach to numerical convection', *J. Comput. Phys.*, **23**, 276–299 (1977).
23. P. L. Roe, 'Some contributions to the modeling of discontinuous flows', *Proc. AMS/SIAM Seminar*, San Diego, CA, 1983.

